Domain Wall Leaky Integrate-and-Fire Neurons With Shape-Based Configurable Activation Functions

Wesley H. Brigner, *Graduate Student Member, IEEE*, Naimul Hassan, *Graduate Student Member, IEEE*, Xuan Hu, *Member, IEEE*, Christopher H. Bennett, *Member, IEEE*, Felipe Garcia-Sanchez, *Member, IEEE*, Can Cui, *Graduate Student Member, IEEE*, Alvaro Velasquez, *Member, IEEE*, Matthew J. Marinella, *Senior Member, IEEE*, Jean Anne C. Incorvia, *Senior Member, IEEE*, and Joseph S. Friedman, *Senior Member, IEEE*

***Abstract*— CMOS devices display volatile characteristics and are not well suited for analog applications such as neuromorphic computing. Spintronic devices, on the other hand, exhibit both non-volatile and analog features, which are well suited to neuromorphic computing. Consequently, these novel devices are at the forefront of beyond-CMOS artificial intelligence applications. However, a large quantity of these artificial neuromorphic devices still require the use of CMOS to implement various neuromorphic functionalities, which decreases the efficiency of the system. To resolve this, we have previously proposed a number of artificial neurons and synapses that do not require CMOS for operation. Although these devices are a significant improvement over previous renditions, their ability to enable neural network learning and recognition is limited by their intrinsic activation functions. This work proposes modifications to these spintronic neurons that enable configuration of the activation functions through control of the shape of a magnetic domain wall track. Linear and sigmoidal activation functions are demonstrated in this work, which can be extended through a similar approach to enable a wide variety of activation functions.**

***Index Terms*— Artificial neural network, leaky integrate-and-fire (LIF) neuron, multilayer perceptron, neuromorphic computing.**

Manuscript received September 24, 2021; revised December 11, 2021 and February 20, 2022; accepted March 8, 2022. Date of publication March 28, 2022; date of current version April 22, 2022. This work was supported in part by the National Science Foundation under Division of Computing and Communication Foundations (CCF) Award 1910800 and Award 1910997, in part by the National Science Foundation Graduate Research Fellowship under Grant 1746053, in part by the Eugene McDermott Graduate Fellowship under Award 202001, and in part by the Texas Analog Center of Excellence Graduate Fellowship. The review of this article was arranged by Editor P. Narayanan. *(Corresponding author: Wesley H. Brigner.)*

Wesley H. Brigner, Naimul Hassan, Xuan Hu, and Joseph S. Friedman are with the Department of Electrical and Computer Engineering, The University of Texas at Dallas, Richardson, TX 75080 USA (e-mail: wesley.brigner@utdallas.edu).

Christopher H. Bennett is with the Sandia National Laboratories, Albuquerque, NM 87213 USA.

Felipe Garcia-Sanchez is with the Department of Applied Physics, University of Salamanca, 37008 Salamanca, Spain.

Can Cui and Jean Anne C. Incorvia are with the Department of Electrical and Computer Engineering, The University of Texas at Austin, Austin, TX 78712 USA.

Alvaro Velasquez is with the Information Directorate, Air Force Research Laboratory, Rome, NY 13441 USA.

Matthew J. Marinella is with the Arizona State University, Tempe, AZ 85281 USA.

Color versions of one or more figures in this article are available at https://doi.org/10.1109/TED.2022.3159508.

Digital Object Identifier 10.1109/TED.2022.3159508

I. Introduction

ACCORDING to neuroscientists, the human brain consists of neurons and synapses. Neurons receive electrical signals through their dendrites and integrate these electrical signals in their somas. When enough input pulses have been received, these cells release output pulses from their somas, through their axons, and into the dendrites of other neurons. Synapses bridge the gaps between two neurons.

Likewise, artificial neuromorphic systems consist of neuron and synapse analogs. They can be implemented using software run on standard von Neumann computers [1], [2], but such a method is highly inefficient due to the fact that conventional mathematical operations do not map efficiently to neuronal and synaptic functions. Furthermore, CMOS technology does not naturally provide the required neuronal or synaptic functionality—instead, these functions must be implemented using a large number of devices per neuron or synapse. The efficiency can be improved by designing CMOS circuitry specifically for neuromorphic applications [3], [4]; however, even though this will significantly reduce the device count, and therefore the power consumption, CMOS devices are still not ideal for these applications due to their volatile and digital nature.

The non-volatility and analog nature of spintronics are particularly attractive for neuromorphic computing, and several beyond-CMOS spintronic synapses and neurons have been proposed to improve the efficiency. Although synapses only require non-volatility and variable resistance, the popular leaky integrate-and-fire (LIF) neuron model requires three primary functionalities: leaking, integrating, and firing. Therefore, while much progress has been made on beyond-CMOS synapses [5]–[8], significant challenges remain to emulate the complex behavior of neurons. Advancing on previous work that required CMOS within the network [8], we have previously proposed spintronic LIF neurons capable of intrinsically providing the three necessary functionalities within a purely spintronic system [9]–[13].

However, these neurons have limited capability to mimic the various activation functions commonly used in neural networks. Activation functions are commonly used in neural networks to improve the decision-making process and, by extension, the learning characteristics of the networks. A variety of activation functions are utilized for neural networks, including the rectified linear unit (ReLU) and squashing/sigmoidal activation functions. Similar activation functions have already been implemented in recent works, but they only implement quantized, not analog, activation functions [14].

In this article, we propose spintronic neurons that provide these activation functions by modifying the shape of one of our previously proposed shape-based magnetic domain wall neurons [11]. By appropriately configuring the shape of this device, it is possible to implement a wide range of distinct activation functions. This permits the design of neural networks that leverage nearly any arbitrary activation function, thereby increasing the efficiency of the spintronic neuromorphic networks.

Section II provides a brief background into the field of neuromorphic computing, including the shape-based neuron. Section III discusses the realization of two particular activation functions, while conclusions are provided in Section IV.

II. Background

Neuromorphic computing is generally realized with neuron layers connected through crossbar synapse arrays. In order to realize the LIF neuron functionality, we have previously proposed the use of artificial spintronic neurons as described in this section. This section also overviews the activation functions of interest for neuromorphic computing.

A. Crossbar Array

Crossbar arrays typically consist of horizontal input wires (word lines) and vertical output wires (bit lines). Input neurons are placed at the inputs to the word lines, and output neurons are placed at the outputs of the bit lines. Synapses, on the other hand, are placed at the intersections of the word and bit lines. Therefore, an $M \times N$ crossbar array will consist of $M + N$ neurons and $M * N$ synapses [15]–[17].

B. LIF Neurons

In order to accurately mimic biological neurons for neuromorphic computing, artificial LIF neurons implement three primary functionalities: leaking, integrating, and firing. When integrating, these neurons accept and store energy from input energy pulses. When no input pulse is provided, the stored energy gradually dissipates. Finally, once sufficient stored energy has been integrated, the neuron releases this energy as an output pulse of its own.

C. Domain Wall-Magnetic Tunnel Junctions

Magnetic tunnel junctions (MTJs) consist of two ferromagnetic layers—a “free” layer capable of changing states and a “fixed” or “pinned” layer whose magnetization is stable. When the two layers are magnetized parallel to each other, the device exhibits a low-resistance state (LRS); when they are magnetized anti-parallel to each other, the device exhibits a high-resistance state (HRS). Domain wall-MTJs (DW-MTJs) are similar, but the free layer is extended and contains two anti-parallel magnetic domains bounded by a domain wall [18], [19]. The DW can be moved with a spin-orbit torque (SOT) current through a heavy metal beneath the DW track or through a spin-transfer torque (STT) current passed through the DW track, and the device changes resistance states when the DW shifts underneath the MTJ.

D. DW-MTJ LIF Neurons

This DW-MTJ device can be used as an LIF as shown in Fig. 1(a), with the neuron energy represented by the position of the DW within the track [9]. Integration is accomplished by applying current through the heavy metal, and firing occurs when the DW passes underneath the MTJ, thereby switching the current across the tunnel barrier. Device resetting can be performed using various methods [20] and is akin to a refractory period.

In order to induce leaking that shifts the DW in the direction opposite the SOT, an energy landscape must be produced that causes the DW to exist in a lower energy state at one end of the device than the other. While this can be achieved by providing current through the DW track in the direction opposite the integration, this approach is undesirable due to the additional control circuitry [8]. It is preferable, therefore, for the leaking to be passive, as in [9]–[12].

The shape-based leaking of [11] is particularly attractive for enabling useful activation functions. With this method, the DW track width is varied from one end of the track to the other, as shown in Fig. 1(b). DWs typically exist in lower energy states in wider tracks than in narrower tracks. Consequently, the variation of the DW track width shown in Fig. 1(b) creates an energy landscape more favorable to the DW existing on the left side of the track than on the right side, causing the DW to shift from right to left. If desired, the leaking speed of the neurons can be increased by increasing w_2 relative to w_1 or by decreasing the Landau–Lifshitz damping, among other methods. Conversely, the leaking speed can be decreased by decreasing w_2 relative to w_1 or by increasing the Landau–Lifshitz damping.

The integrating and leaking characteristics observed in mumax3 micromagnetic simulations are illustrated in Fig. 1(c) [11]. The magnetic parameters are listed in Table I. These micromagnetic parameters are used for the entirety of this work, including the linear and squashing neurons of Section III. Throughout this work, COMSOL has been used

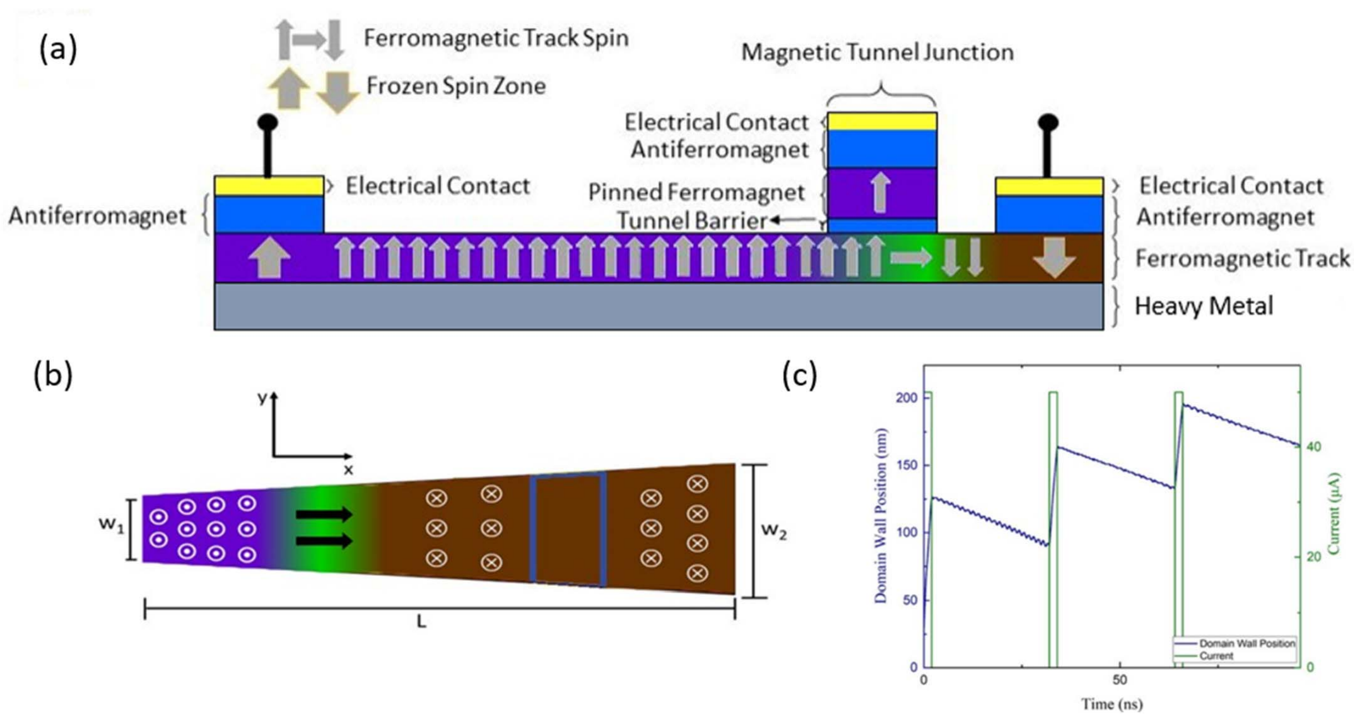

Fig. 1. (a) Side view of a DW-MTJ neuron. (b) Top view of the neuron with shape-based DW drift. (c) Combined integrating and leaking characteristics of a shape-based DW drift neuron with $L = 250$ nm, $w_1 = 50$ nm, and $w_2 = 100$ nm, where the current is applied from right to left through the DW track using the left and right terminals.

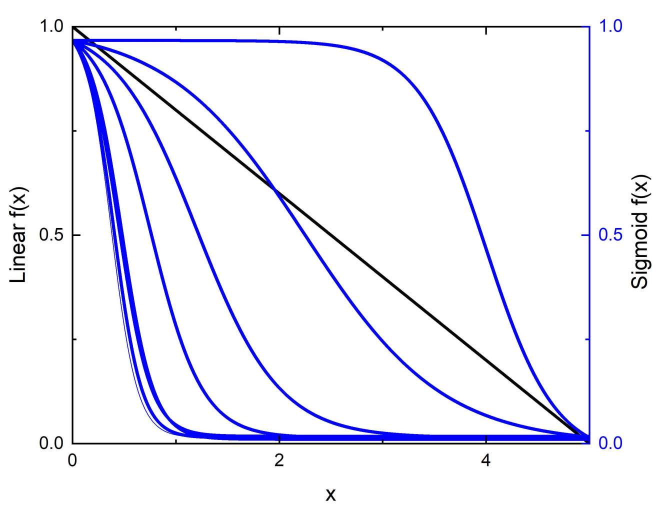

Fig. 2. Generalized linear (black) and sigmoidal (blue) activation functions. The sigmoidal activation functions are shown with various switching speeds.

to create a current map for non-rectangular DW-MTJ neuron structures.

E. Activation Functions

Activation functions allow a neuron to provide the network with significantly improved learning characteristics during training and significantly improved performance during operation. In fact, it has been shown that particular activation functions, such as the ReLU or sigmoidal activation functions shown in Fig. 2, can reduce the error exhibited by a neural network by up to two orders of magnitude when the network is applied to certain datasets.

The ReLU activation function simply maps an input to the output in a linear fashion. On the other hand, the sigmoid function (also referred to as the squashing function) maps the input to a monotonically decreasing output, with the highest rate of change at the center of the function. Table II provides the equations representing these activation functions.

As an activation function describes the impact of the stimuli input to a neuron on the stimuli output by a neuron, the activation function of an LIF neuron is a complex function dependent on the history of input stimuli. Although conventional activation functions used in machine learning can be characterized by equations that directly relate the input

TABLE I
MATERIAL PARAMETERS

Symbol	Parameter	Value
A_{ex}	Exchange Stiffness [J/m]	1.3×10^{-12}
α	Landau-Lifshitz Damping Constant [dimensionless]	0.05
ξ	Non-Adiabaticity of STT [dimensionless]	0.05
M_{sat}	Saturation Magnetization [A/m]	7.96×10^5
Ku	First Order Uniaxial Anisotropy Constant [J/m^3]	5×10^5

Material parameters used in the micromagnetic simulations. The parameters shown here correspond to those exhibited by CoFeB.

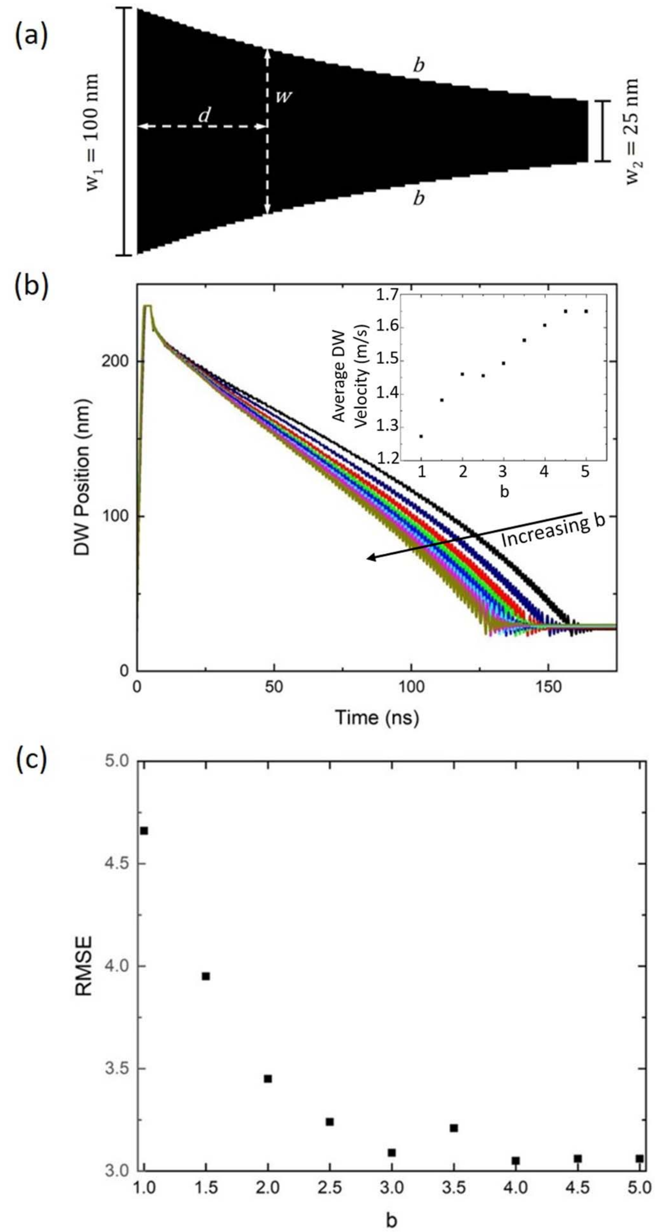

Fig. 3. (a) Top view of the linear neuron, displaying the slight exponential curvature of the sides of the track. This curvature is of the form $w \propto b^{-d}$, where b represents the curvature of the sides, d is the distance from the wide end of the track in nanometer, and w is the width of the device in nanometer at distance d. b ranges from 1 to 5 at intervals of 0.5. When $b = 1$, the sides are straight, and the track is identical to the one shown in Fig. 1(b). (b) Leaking characteristics of the linear neuron for various values of b, including $b = 1$. (Inset) Average DW velocity in m/s as a function of b. (c) RMSE of the neuron's leaking characteristics from a linear function.

and output signals, the activation function of an LIF neuron has time-dependent behavior that cannot be expressed by such simple functions. However, by modifying the leaking, integrating, or firing behavior of an LIF neuron, the activation function of the LIF neuron is altered. In particular, as explained in [21], an activation function can be described by a saturation function, which, for an LIF neuron, is equivalent to integration. This work, therefore, investigates the configurability of LIF neuron activation functions through control of the neuron structures that govern the leaking and integration behavior.

TABLE II
ACTIVATION FUNCTION EQUATIONS

Function	Form	Value a	Value b
Linear	$f(x) = ax + b$	-1	1
Sigmoid	$f(x) = \dfrac{1}{1 + e^{a(x-b)}}$	10	2.25
		15	1.2
		15	0.75
		15	0.475
		15	0.45
		15	0.4
		15	0.4
		15	0.375

Equations representing the activation functions in Fig. 2.

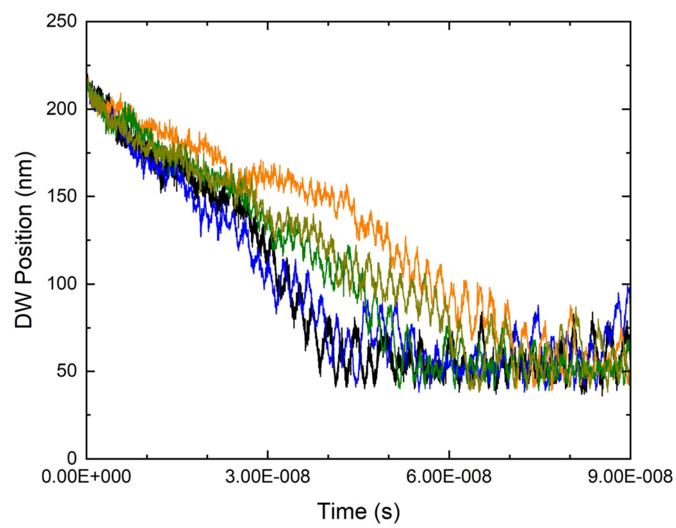

Fig. 4. Simulation of a linear neuron with $b = 4$ at 300 K with five randomly generated seeds.

III. DW-MTJ NEURONS WITH CONFIGURABLE ACTIVATION FUNCTIONS

In order to improve the biomimetic capabilities of our neurons, it is important for them to implement a variety of activation functions, including the linear and squashing activation functions [22]–[26]. To do so, modifications to the neurons are required. The neuron from [11] is particularly well suited to implementing these functions due to the simplicity of the necessary changes. Although this section only demonstrates the linear and squashing activation functions, it is clear that this approach can be extended to a wide variety of activation functions using similar modifications.

It is important to note that while the leaking behavior is dependent solely on the neuron structure, the integration behavior is also dependent on the applied input current magnitude. Therefore, in order to ensure that the desired activation functions are always significantly impacting the neuron behavior, these activation functions are implemented in terms of the leaking rather than the integration. For any given leaking activation function, a wide range of integration activation functions can be achieved by varying the current magnitude applied to the DW-MTJ neuron.

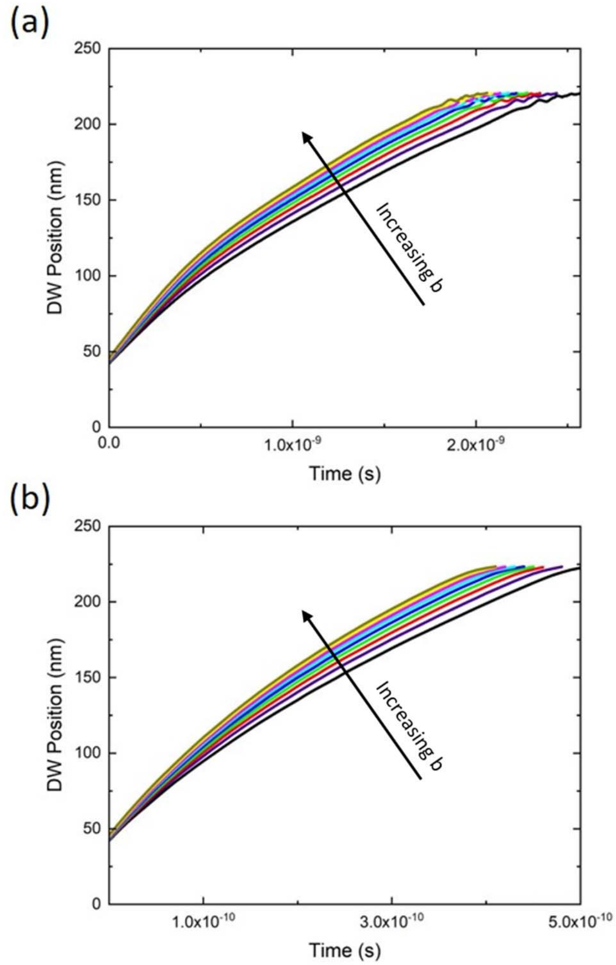

Fig. 5. (a) Integration of the linear neuron for an input current of 0.1 mA. As with Fig. 4(b), b ranges from 1 to 5 with an increment of 0.5. (b) Integration of the linear neuron for an input current of 0.5 mA.

A. Neuron With Linear Activation Function

In the trapezoidal DW-MTJ device of Fig. 1(b), the DW accelerates as it nears the narrow end of the track. To realize a linear activation function without this acceleration, it is necessary to alter the shape of the DW track to decrease the leaking force in narrower regions of the track.

Linear leaking can be accomplished simply by introducing a slight exponential variation in the width of the DW track, as shown in Fig. 3. In general, as the value of b increases, the linearity of the device's leaking increases, calculated as the inverse of the root mean squared error (RMSE) of a linear regression performed on the leaking curve. The leaking speed also increases as b increases. However, once b reaches a certain point, further increases cease to produce an increase in linearity, although they continue to increase the leaking speed. This exponential variation decreases the leaking force applied to the domain wall as it shifts to narrower regions of the track, preventing further DW acceleration and allowing for linear device operation. Additionally, the room temperature leaking characteristics of the neuron with $b = 4$ are illustrated in Fig. 4, demonstrating robustness to temperature.

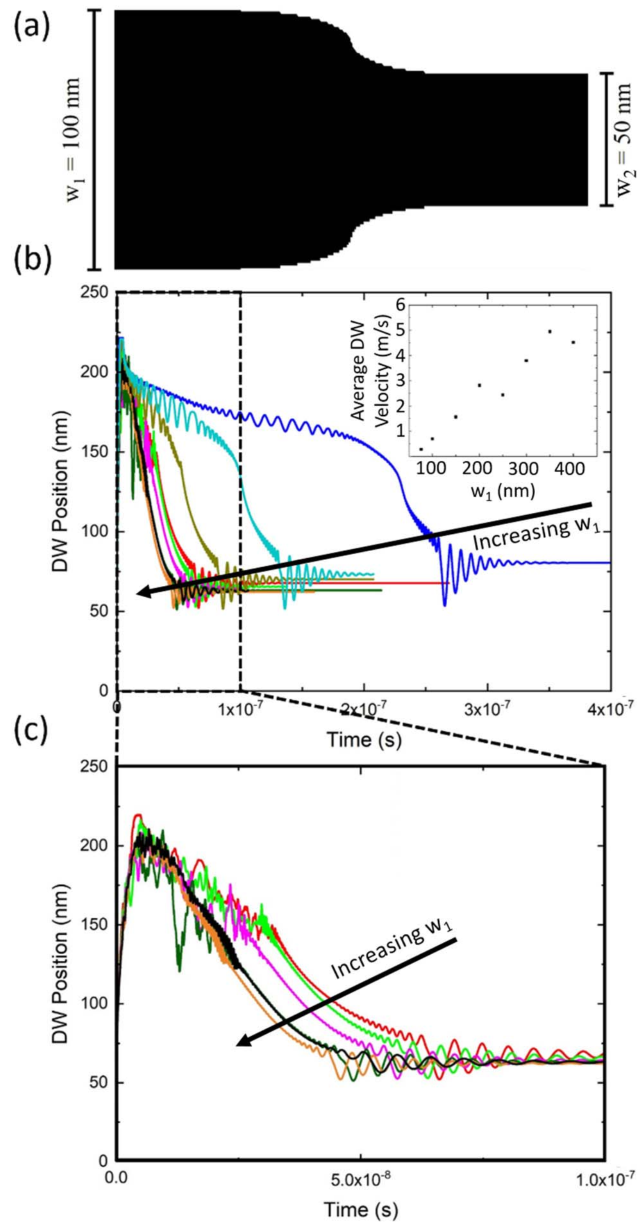

Fig. 6. (a) Top view of the squashing neuron, displaying the sharp constriction of the DW track centered in the middle of the track. (b) Leaking characteristics of the squashing neuron for w_1 increasing from 100 to 400 nm, with an increment of 50 nm. (Inset) Average DW velocity in m/s as a function of w_1 in nanometer. (c) Leaking characteristics of the squashing neuron for w_1 increasing from 150 to 400 nm, into the time range 0 s–100 ns.

It is also important to analyze the response of the DW-MTJ neurons to various input currents. When an input current of 0.1 mA is applied to the neuron, as in Fig. 5(a), the DW's integration speed increases in proportion to b. As the DW nears the end of its range of motion, it also begins to exhibit slight oscillatory behavior due to interactions with the fixed region at the edge of the neuron. When the input current is increased to 0.5 mA, as shown in Fig. 5(b), the integration speed also increases, as would be expected. Additionally, the integration speed maintains its positive correlation with the value of b, but the higher current prevents the previously observed oscillations of the DW at the edges of its range of motion.

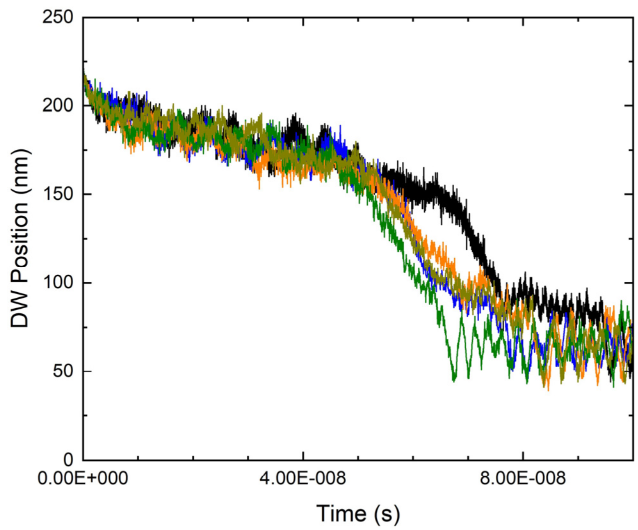

Fig. 7. Simulation of a linear neuron with $w = 150$ at 300 K with five randomly generated seeds.

B. Neuron With Squashing Activation Function

In order to implement sigmoidal leaking, the leaking force must not only be minimized at the narrow end of the track, but also at the wide end of the track. Therefore, the neuron's shape gradient can only exist within a narrow range halfway between the narrow and wide ends of the DW track, as illustrated in Fig. 6(a).

With $w_1 = 100$ nm as in Fig. 6(b), the neuron exhibits a sigmoidal leaking characteristic. As the width of the wide end of the track increases, the DW leaking motion becomes faster, with an effect similar to that of b on the leaking speed of a linear neuron. By zooming in on the leaking characteristics for these larger values of w_1 in Fig. 6(c), it can be observed that the neurons still implement squashing functions. By varying the device width in this fashion, low leaking forces are applied to the DW in both the wide and narrow regions and higher leaking forces are applied to the DW in the middle region, causing the device to exhibit sigmoidal characteristics. As with the linear neurons, the room temperature leaking characteristics for a device with $w_1 = 150$ nm are illustrated in Fig. 6. As with the linear neuron, the room temperature leaking characteristics of the neuron with $w_1 = 150$ nm are illustrated in Fig. 7, demonstrating robustness to temperature.

As with the previously discussed linear neuron, it is important to analyze the integration characteristics of the squashing neurons for various input currents. With an input current of 0.1 mA, as illustrated in Fig. 8(a), the DW integration speed is inversely proportional to w_1, partly due to an increased leaking force and partly due to a decreased current density. Additionally, as the width increases, the integration becomes non-monotonic due to the instability of the wide DWs. When the input current is increased to 0.5 mA as in Fig. 8(b), not only does the DW integration speed increase significantly, the integration speed remains inversely related to w_1. Additionally, with increased current, the integration becomes monotonic even with large widths.

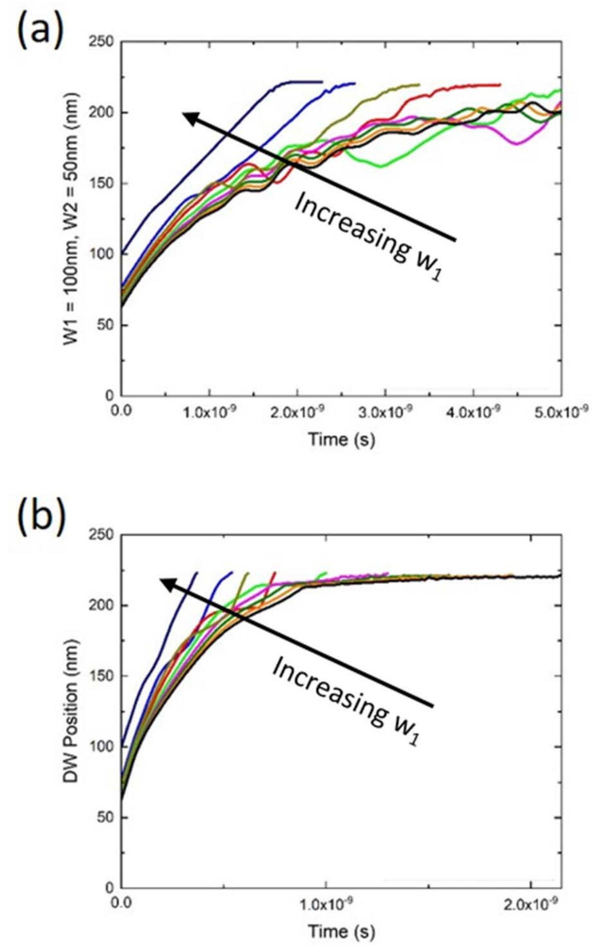

Fig. 8. (a) Integration of the squashing neuron with an input current of 0.1 mA. (b) Integration of the squashing neuron with an input of 0.5 mA. As w_1 increases, the steady-state fully leaked initial position approaches the end of the track.

IV. Conclusion

Shape-based DW drift enables configurable DW-MTJ neuron leaking that enables the realization of diverse activation functions for efficient learning and recognition in spintronic neuromorphic computing systems. In this work, we have demonstrated linear and squashing activation functions through specific configurations of the shape of the DW tracks. By extension of this concept, further activation functions commonly used in the field of neuromorphic can also be realized. This represents a significant advancement over previous spintronic neurons that will enable drastically improved learning characteristics of spintronic neural networks.

Acknowledgment

The authors thank E. Laws, J. McConnell, N. Nazir, L. Philoon, and C. Simmons for technical support, and the Texas Advanced Computing Center at The University of Texas at Austin, Austin, TX, USA, for providing computational resources. Sandia National Laboratories, Albuquerque, NM, USA, is a multimission laboratory managed and operated by National Technology and Engineering Solutions of Sandia, LLC, Albuquerque, a wholly owned subsidiary of Honeywell International Inc., for the U.S. Department of Energy's

National Nuclear Security Administration under Contract DE-NA0003525. This article describes objective technical results and analysis. Any subjective views or opinions that might be expressed in the article do not necessarily represent the views of the U.S. Department of Energy or the United States Government.

References

[1] A. Delorme, J. Gautrais, R. van Rullen, and S. J. Thorpe, "SpikeNet: A simulator for modeling large networks of integrate and fire neurons," *Neurocomputing*, vols. 26–27, pp. 989–996, Jun. 1999.

[2] S. Han, H. Mao, and W. J. Dally, "Deep compression: Compressing deep neural networks with pruning, trained quantization and Huffman coding," in *Proc. ICLR*, 2016. [Online]. Available: https://dblp.org/db/conf/iclr/iclr2016.html

[3] F. Akopyan *et al.*, "TrueNorth: Design and tool flow of a 65 mW 1 million neuron programmable neurosynaptic chip," *IEEE Trans. Comput.-Aided Design Integr. Circuits Syst.*, vol. 34, no. 10, pp. 1537–1557, Oct. 2015.

[4] P. A. Merolla *et al.*, "A million spiking-neuron integrated circuit with a scalable communication network and interface," *Science*, vol. 345, no. 6197, pp. 668–673, 2014.

[5] D. B. Strukov, G. S. Snider, D. R. Stewart, and R. S. Williams, "The missing memristor found," *Nature*, vol. 453, pp. 80–83, May 2008.

[6] X. Chen *et al.*, "A compact skyrmionic leaky–integrate–fire spiking neuron device," *Nanoscale*, vol. 10, no. 13, pp. 6139–6146, 2018.

[7] S. Dutta, S. A. Siddiqui, F. Buttner, L. Liu, C. A. Ross, and M. A. Baldo, "A logic-in-memory design with 3-terminal magnetic tunnel junction function evaluators for convolutional neural networks," in *Proc. IEEE/ACM Int. Symp. Nanoscale Archit. (NANOARCH)*, Jul. 2017, pp. 83–88.

[8] A. Sengupta, Y. Shim, and K. Roy, "Proposal for an all-spin artificial neural network: Emulating neural and synaptic functionalities through domain wall motion in ferromagnets," *IEEE Trans. Biomed. Circuits Syst.*, vol. 10, no. 6, pp. 1152–1160, May 2016.

[9] N. Hassan *et al.*, "Magnetic domain wall neuron with lateral inhibition," *J. Appl. Phys.*, vol. 124, no. 15, Oct. 2018, Art. no. 152127.

[10] W. H. Brigner *et al.*, "Graded-anisotropy-induced magnetic domain wall drift for an artificial spintronic leaky integrate-and-fire neuron," *IEEE J. Explor. Solid-State Computat. Devices Circuits*, vol. 5, no. 1, pp. 19–24, Jun. 2019.

[11] W. H. Brigner *et al.*, "Shape-based magnetic domain wall drift for an artificial spintronic leaky integrate-and-fire neuron," *IEEE Trans. Electron Devices*, vol. 66, no. 11, pp. 4970–4975, Nov. 2019.

[12] W. H. Brigner *et al.*, "Three artificial spintronic leaky integrate-and-fire neurons," *SPIN*, vol. 10, no. 2, Jun. 2020, Art. no. 2040003.

[13] W. H. Brigner *et al.*, "CMOS-free multilayer perceptron enabled by four-terminal MTJ device," 2020, *arXiv:2002.00862*.

[14] S. A. Siddiqui, S. Dutta, A. Tang, L. Liu, C. A. Ross, and M. A. Baldo, "Magnetic domain wall based synaptic and activation function generator for neuromorphic accelerators," *Nano Lett.*, vol. 20, no. 2, pp. 1033–1040, Feb. 2020.

[15] Y.-P. Lin *et al.*, "Physical realization of a supervised learning system built with organic memristive synapses," *Sci. Rep.*, vol. 6, no. 1, p. 31932, Oct. 2016.

[16] C. H. Bennett, J. A. C. Incorvia, X. Hu, N. Hassan, J. S. Friedman, and M. M. Marinella, "Semi-supervised learning and inference in domain-wall magnetic tunnel junction (DW-MTJ) neural networks," *Proc. SPIE*, vol. 11090, Sep. 2019, Art. no. 110903I.

[17] M. Sharad, D. Fan, K. Aitken, and K. Roy, "Energy-efficient non-Boolean computing with spin neurons and resistive memory," *IEEE Trans. Nanotechnol.*, vol. 13, no. 1, pp. 23–34, Jan. 2014.

[18] J. A. Currivan-Incorvia *et al.*, "Logic circuit prototypes for three-terminal magnetic tunnel junctions with mobile domain walls," *Nature Commun.*, vol. 7, no. 1, Apr. 2016, Art. no. 010275.

[19] J. A. Currivan, Y. Jang, M. D. Mascaro, M. A. Baldo, and C. A. Ross, "Low energy magnetic domain wall logic in short, narrow, ferromagnetic wires," *IEEE Magn. Lett.*, vol. 3, 2012, Art. no. 3000104.

[20] S. Liu, C. H. Bennett, J. S. Friedman, M. J. Marinella, D. Paydarfar, and J. A. C. Incorvia, "Controllable reset behavior in domain wall–magnetic tunnel junction artificial neurons for task-adaptable computation," *IEEE Magn. Lett.*, vol. 12, 2021, Art. no. 4500805.

[21] W. Maass, "Networks of spiking neurons: The third generation of neural network models," *Neural Netw.*, vol. 10, no. 9, pp. 1659–1671, 1997.

[22] K. He, X. Zhang, S. Ren, and J. Sun, "Delving deep into rectifiers: Surpassing human-level performance on ImageNet classification," 2015, *arXiv:1502.01852*.

[23] A. H. Namin, K. Leboeuf, R. Muscedere, H. Wu, and M. Ahmadi, "Efficient hardware implementation of the hyperbolic tangent sigmoid function," in *Proc. IEEE Int. Symp. Circuits Syst.*, May 2009, pp. 2117–2120.

[24] I. Tsmots, O. Skorokhoda, and V. Rabyk, "Hardware implementation of sigmoid activation functions using FPGA," in *Proc. IEEE 15th Int. Conf. Exper. Designing Appl. CAD Syst. (CADSM)*, Feb. 2019, pp. 34–38.

[25] K. Leboeuf, A. H. Namin, R. Muscedere, H. Wu, and M. Ahmadi, "High speed VLSI implementation of the hyperbolic tangent sigmoid function," in *Proc. 3rd Int. Conf. Converg. Hybrid Inf. Technol.*, Nov. 2008, pp. 1070–1073.

[26] A. C. Marreiros, J. Daunizeau, S. J. Kiebel, and K. J. Friston, "Population dynamics: Variance and the sigmoid activation function," *NeuroImage*, vol. 42, no. 1, pp. 147–157, Aug. 2008.